Table 3

Protein components in monkey drusen

Protein	Accession No.	Protein	Accession No.
Actin, α 2	gi|4501883|	**Hemoglobin, β**	gi|4504349|
Albumin	gi|4502027|	*Hemoglobin, delta*	gi|70353|
Aldehyde dehydrogenase 3	gi|283971|	*Histone, H2A C*	gi|4504239|
Aldehyde dehydrogenase 5	gi|105247|	*Histone, H2A Z*	gi|4504255|
Aldolase A	gi|4557305|	*Histone, H2B F*	gi|10800140|
Alpha-1-antitrypsin	gi|1703025|	*Ig, α 2C*	gi|113585|
Alpha-1B-Glycoprotein	gi|46577680|	**Ig, gamma 2C**	gi|121043|
Annexin V	gi|4502107|	**Ig, lambda**	gi|87890|
Apolipoprotein E	gi|4557325|	Lactate dehydrogenase A	gi|5031857|
ATP synthase α chain, mitochondrial	gi|4757810|	Malate dehydrogenase 1	gi|5174539|
Calmodulin 2	gi|4502549|	Peptidylprolyl isomerase A isoform 1	gi|10863927|
Calreticulin	gi|4757900|	Phosphoglycerate kinase 1	gi|4505763|
cAMP-dependent protein kinase inhibitor, β	gi|14210480|	Phosphoinositide 3-kinase, T96	gi|7434348|
Cell adhesion protein SQM1	gi|105595|	Plectin 1	gi|14195007|
Ceruloplasmin	gi|4557485|	Prostatic binding protein	gi|4505621|
Clusterin	gi|4502905|	Protease inhibitor 4	gi|21361302|
Collagen, α 1(VII)	gi|627406|	Pyruvate dehydrogenase	gi|4885543|
Complement component 5	gi|4502507|	Pyruvate kinase, M1 isozyme	gi|20178296|
Complement component 9	gi|4502511|	Ran binding Protein 2	gi|1709217|
Creatine kinase B	gi|125294|	Recoverin	gi|4506459
Crystallin, β B2	gi|299263|	Retinol binding protein 3	gi|4506453|
Crystallin, β S	gi|345764|	Structural maintenance of chromosomes 1-like 1	gi|30581135|
Dystrobrevin, α isoform 8	gi|14916515|	Transferrin	gi|4557871|
Enolase 2	gi|5803011|	Triosephosphate isomerase 1	gi|4507645|
G3PDH	gi|7669492	*Tubulin, α 3*	gi|5174733|
Glucose phosphate isomerase	gi|18201905|	Ubiquitin and ribosomal protein L40	gi|4507761|
Glutamate-ammonia ligase	gi|2144562|	Ubiquitous mitochondrial creatine kinase	gi|10334859|
Haptoglobin	gi|4826762|	**Vimentin**	gi|14742600|
Haptoglobin-related protein	gi|123510|	**Vitronectin**	gi|72146|
Hemoglobin, α 2	gi|4504345|	14-3-3 protein β/α	gi|4507949|

The components consistent with those of AMD drusen are shown in bold letters. The components that belong to the gene families, other members of which are known to be constituents of drusen in AMD, are shown in italic letters. National Center for Biotechnology Information database accession and version numbers are listed.

Fig. 1

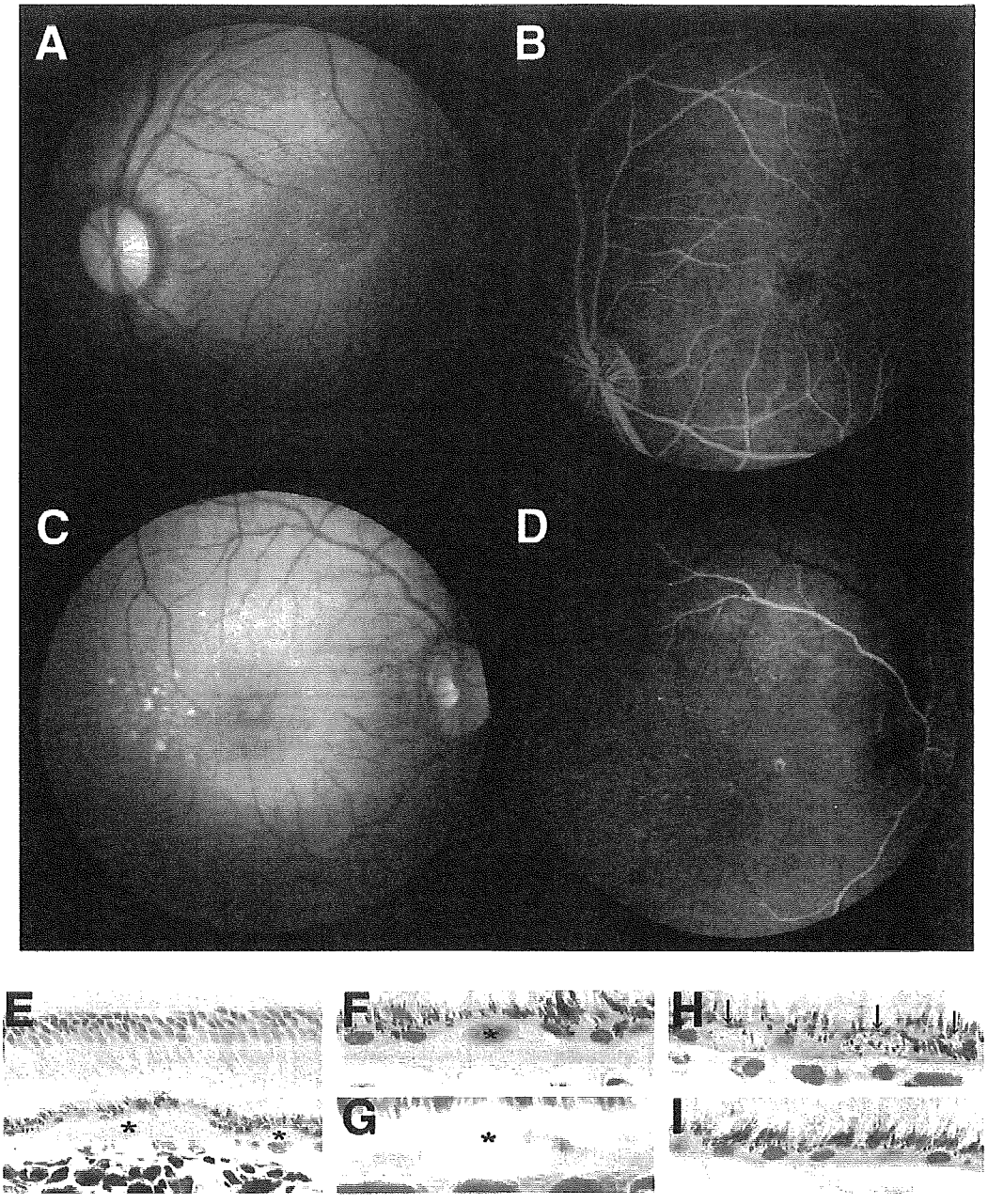

Figure 1. Drusen and degenerative changes of the RPE cells in late onset macular degeneration monkeys. Fundus photographs (*A*, *C*) and fluorescein angiography (FA) (*B*, *D*) of monkeys affected with late onset macular degeneration. Fine dots colored in yellowish-white could be observed in maculae (*A*, *C*). Hyperfluorescein dots could be detected by FA corresponding to these spots (*B*, *D*). Fundus photograph and FA of a 17-year-old monkey that showed vacuolation and hyper- or hypopigmentation of the RPE cells (*A*, *B*). The fundus photograph and FA of another 17-year-old monkey that showed drusen (*C*, *D*). No abnormalities were found in the optic disc nor the blood vessels. *E*) Various sized drusen accumulated between the RPE and choriocapillaris in the macular region (asterisks). Photoreceptor inner and outer segments appeared largely normal. *F*) Drusen that had an eosinophilic inclusion (asterisk). *G*) This spherical structure showed equivalent autofluorescence to that emitted by lipofuscin granules in the RPE (asterisk). *H*) Vacuolation and hyper- or hypopigmentation of the RPE cells (arrows). *I*) Intact region of the RPE in the same monkey as *H*.

Fig. 2

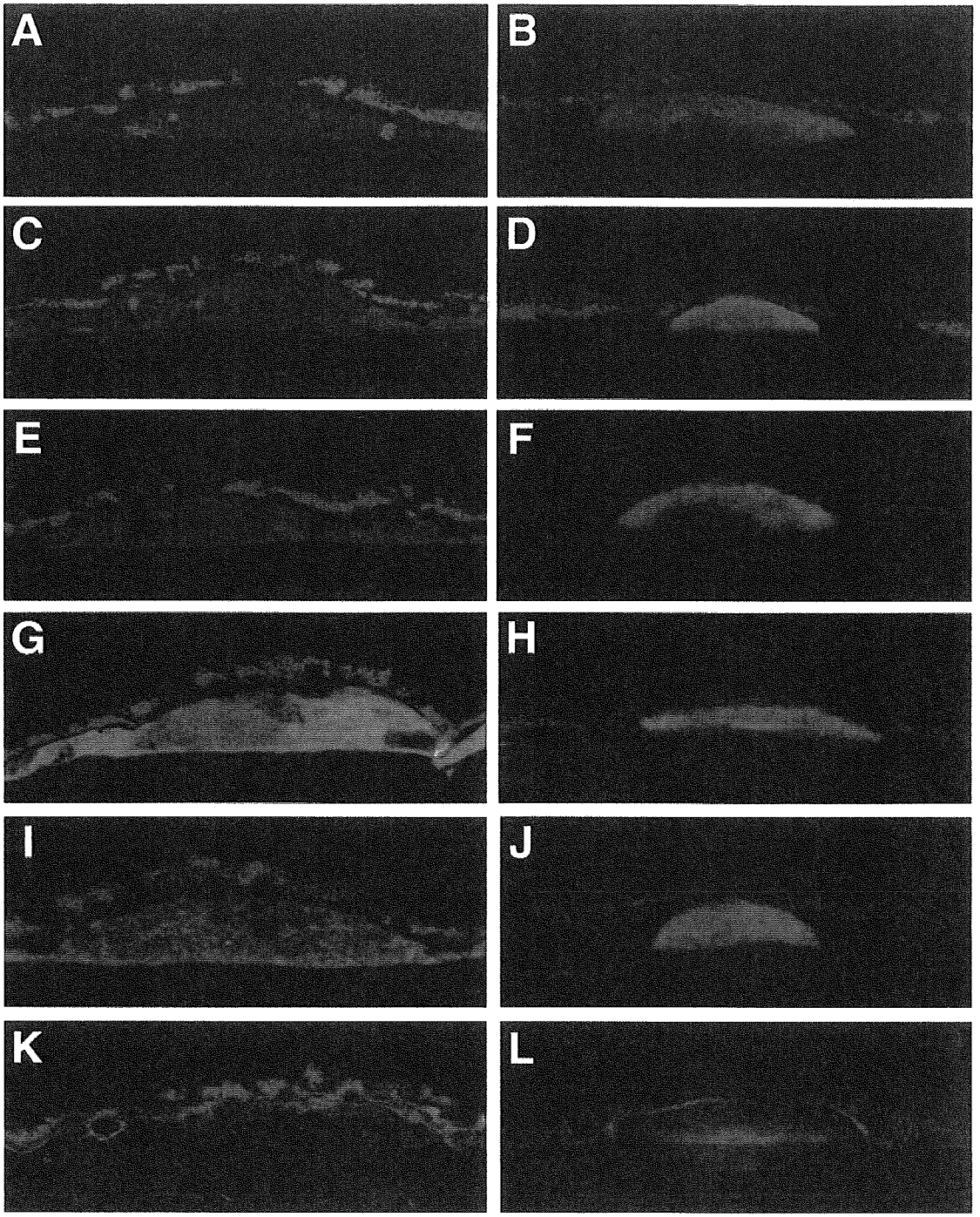

Figure 2. Drusen both in late onset and early onset macular degeneration monkeys are immun-reactive for protein components known in human AMD. Drusen in late onset (*A*, *C*, *E*, *G*, *I*, *K*) and early onset (*B*, *D*, *F*, *H*, *J*, *L*) macular degeneration were heterogeneously bound by antibodies directed against apolipoprotein E (*A, B*), amyloid P component (*C, D*), complement component C5 (*E*, *F*), the terminal C5b-9 complement complex (*G*, *H*), vitronectin (*I*, *J*), and membrane cofactor protein (*K*, *L*). Double-labeled images were generated by the green channel for each antigen and red channel for autofluorescence emitted by lipofuscin pigment in the RPE.

Fig. 3

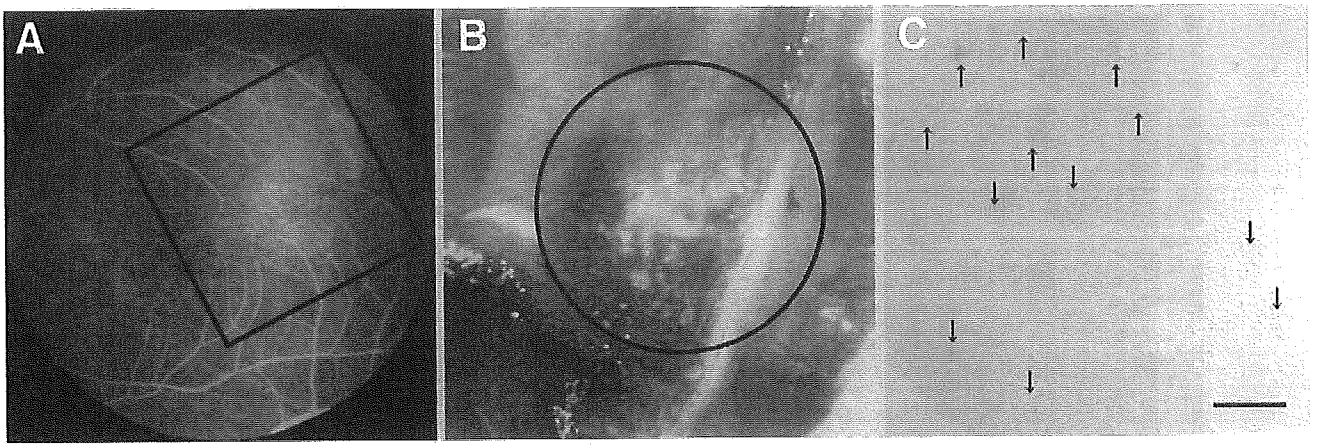

Figure 3. Isolation of drusen. ***A***) FA photograph of a monkey retina used for drusen isolation. A number of drusen that show hyperfluorescence could be observed in parafoveal region (indicated by a rectangle). ***B***) Drusen could be observed attached to surface of Bruch's membrane at magnifications between 20 and 30 diameters under a stereoscopic microscope (white materials in a circle). ***C***) Isolated drusen (arrows). Diameter of a circle in ***B*** = 3 mm. Bar in ***C*** = 1 mm.

Fig. 4

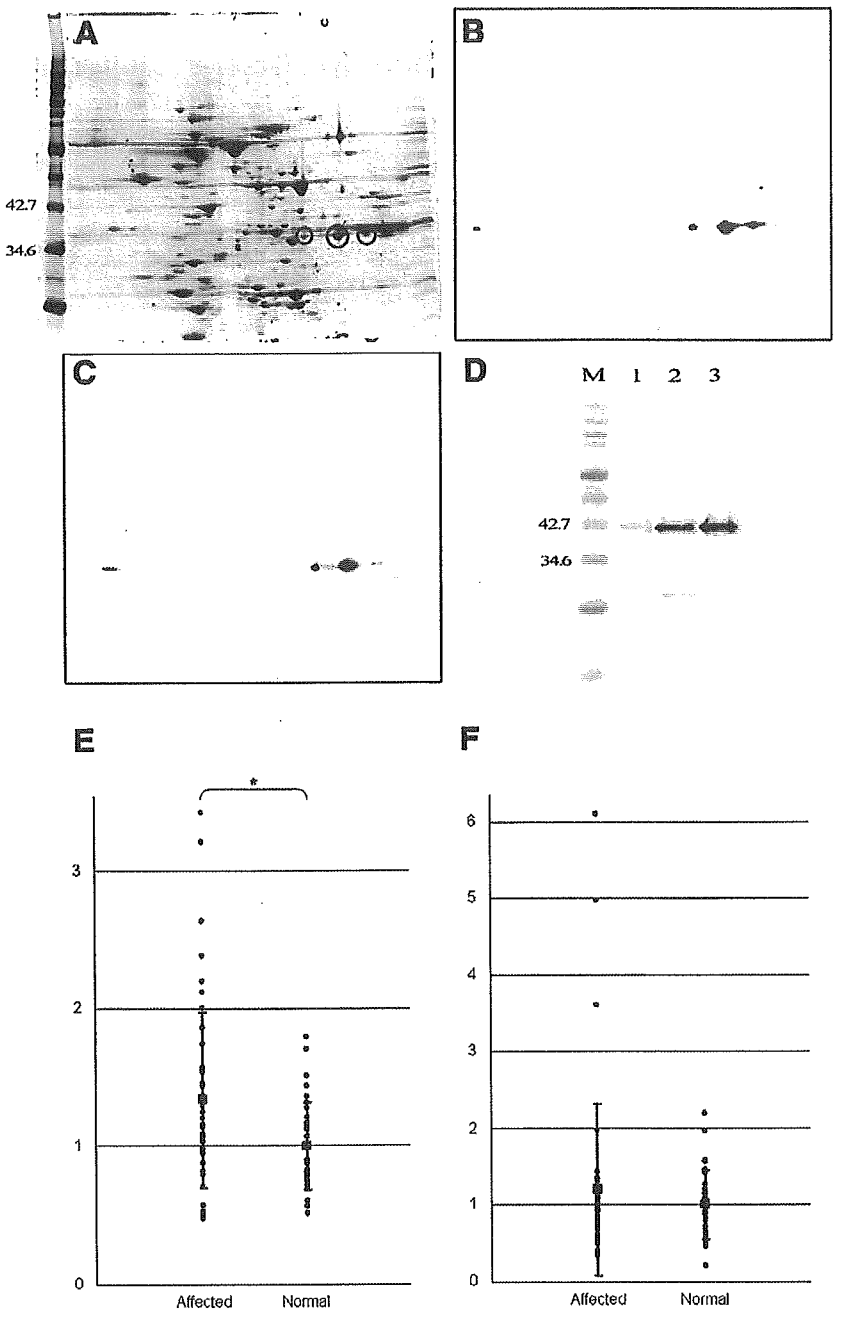

Figure 4. Identification of immunogenic molecules for autoantibodies in the affected monkey sera with late onset macular degeneration. ***A***) 2-D electrophoretic image of retinal proteins visualized by SYPRO Ruby. ***B***) Serum from same monkey in **Fig. 1*C*** showed 3 immunoreactive spots in a row at ~38 kDa. Corresponding protein spots to chemiluminescent signals were excised (circles in ***A***) and analyzed by LC-MS/MS. ***C***) Chemiluminescent signals obtained by immunoreaction with anti-annexin II monoclonal antibodies completely matched those with the serum. ***D***) The affinity purified recombinant annexin ran on SDS-PAGE gel at ~41 kDa (lane 1). Recombinant proteins reacted with both anti-annexin II monoclonal antibodies (lane 2) and autoantibodies in serum (lane 3). M, molecular size marker (kDa). Relative antibody titers against annexin II (***E***) or μ-crystallin (***F***) in sera from affected monkeys with late onset macular degeneration and age-matched control animals. Relative antibody titers of individual monkeys are indicated by ratio to mean of normal monkeys. **P* value <0.01.

Fig. 5

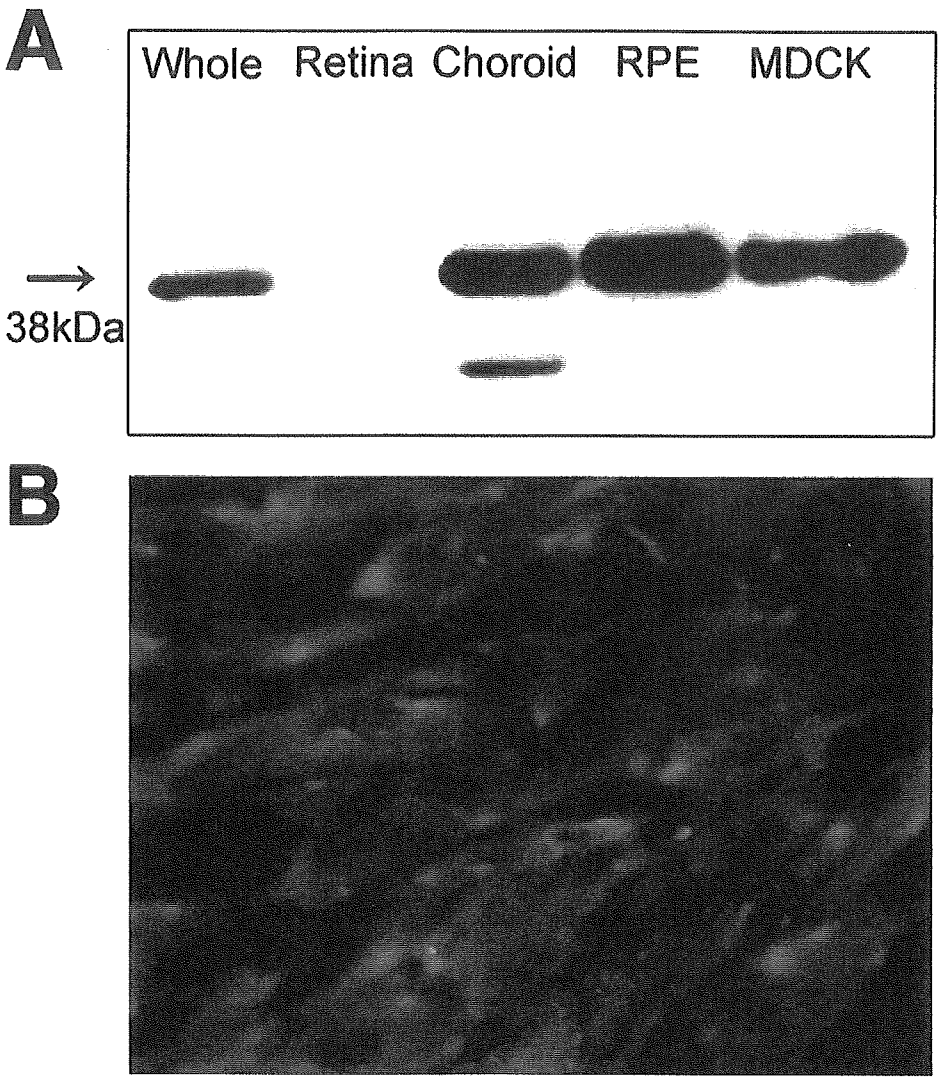

Figure 5. Expression of annexin II in the retina. ***A***) Protein expression of annexin II (38 kDa) was confirmed in whole retina, choroid, and most intensively in cultured human RPE cells. Protein extract from MDCK cells was used for positive control. ***B***) Fluorescence microscopy demonstrated that RPE cells highly expressed annexin II in vitro.

STEM CELLS®
Original Article

Repair of Infarcted Myocardium Mediated by Transplanted Bone Marrow–Derived CD34+ Stem Cells in a Nonhuman Primate Model

TORU YOSHIOKA[a,c] NAOHIDE AGEYAMA,[f] HIROAKI SHIBATA,[a,f] TAKANORI YASU,[c] YOSHIO MISAWA,[d] KOICHI TAKEUCHI,[e] KEIJI MATSUI,[c] KEIJI YAMAMOTO,[c] KEIJI TERAO,[f] KAZUYUKI SHIMADA,[c] UICHI IKEDA,[g] KEIYA OZAWA,[a,b] YUTAKA HANAZONO[a]

[a]Center for Molecular Medicine; [b]Division of Hematology, and [c]Division of Cardiology, Department of Internal Medicine; [d]Division of Cardiovascular Surgery, Department of Surgery; and [e]Department of Anatomy, Jichi Medical School, Minamikawachi, Tochigi; [f]Tsukuba Primate Center, National Institute of Infectious Diseases, Tsukuba, Ibaraki; [g]Department of Organ Regeneration, Shinshu University Graduate School of Medicine, Matsumoto, Nagano, Japan

Key Words. Nonhuman primate • Acute myocardial infarction • Stem cell transplantation Genetic marking • Lentivirus vector • Plasticity • Neoangiogenesis

ABSTRACT

Rodent and human clinical studies have shown that transplantation of bone marrow stem cells to the ischemic myocardium results in improved cardiac function. In this study, cynomolgus monkey acute myocardial infarction was generated by ligating the left anterior descending artery, and autologous CD34+ cells were transplanted to the peri-ischemic zone. To track the in vivo fate of transplanted cells, CD34+ cells were genetically marked with green fluorescent protein (GFP) using a lentivirus vector before transplantation (marking efficiency, 41% on average). The group receiving cells ($n = 4$) demonstrated improved regional blood flow and cardiac function compared with the saline-treated group ($n = 4$) at 2 weeks after transplant. However, very few transplanted cell–derived, GFP-positive cells were found incorporated into the vascular structure, and GFP-positive cardiomyocytes were not detected in the repaired tissue. On the other hand, cultured CD34+ cells were found to secrete vascular endothelial growth factor (VEGF), and the in vivo regional VEGF levels showed a significant increase after the transplantation. These results suggest that the improvement is not the result of generation of transplanted cell–derived endothelial cells or cardiomyocytes; and raise the possibility that angiogenic cytokines secreted from transplanted cells potentiate angiogenic activity of endogenous cells.
STEM CELLS *2005;23:355–364*

INTRODUCTION

Recent clinical studies have shown that the introduction of bone marrow cells can restore blood flow in ischemic myocardium and ameliorate cardiac function [1–6]. Despite enthusiasm for these studies, it is unclear how transplanted bone marrow cells contribute to the clinical improvement. Because endothelial progenitor cells are identified in bone marrow cells [7], these cells might participate in the repair

Correspondence: Yutaka Hanazono, M.D., Ph.D., Division of Regenerative Medicine, Center for Molecular Medicine, Jichi Medical School, 3311-1 Yakushiji, Minamikawachi, Tochigi 329-0498, Japan. Telephone: 81-285-58-7450; Fax: 81-285-44-5205; e-mail: hanazono@jichi.ac.jp Received August 16, 2004; accepted for publication November 30, 2004. ©AlphaMed Press 1066-5099/2005/$12.00/0 doi: 10.1634/stemcells.2004-0200

of vascular tissue. On the other hand, it has been reported that hematopoietic stem cells differentiate into endothelial cells and cardiomyocytes when transplanted into the ischemic myocardium in mice [8]. More recently, however, it has been reported that hematopoietic stem cells do not give rise to nonhematopoietic cells in the ischemic myocardium in murine models [9–11].

In vivo tracking and plastic properties of hematopoietic stem or progenitor cells have not been examined in primate cardiac ischemia. We have transplanted genetically marked autologous CD34+ cells to the ischemic myocardium in a nonhuman primate (cynomolgus macaque) model and tracked the in vivo fate of the cells. We have used CD34+ cells because the cells are widely used as a fraction of hematopoietic stem cells in clinical and nonhuman primate studies [12]. In addition, CD34+ cells contain vascular endothelial progenitor cells [7]. Thus, the present study can address the question of whether transplanted CD34+ cells really give rise to endothelial cells and cardiomyocytes in ischemic myocardium in primates.

Materials and Methods

Animals

Eight cynomolgus macaques bred in the Tsukuba Primate Center (Ibaraki, Japan) were enrolled in the present study. This study strictly adhered to the rules for animal care and management of the Tsukuba Primate Center, as well as the guiding principles for animal experiments using nonhuman primates formulated by the Primate Society of Japan. The protocols of animal experiments were approved by the animal welfare and animal care committee of the National Institute of Infectious Diseases (Tokyo).

Preparation of CD34+ Cells

Cynomolgus bone marrow (50 ml) was aspirated from the iliac crest under an isoflurane-induced general anesthesia. From the bone marrow, a nucleated cell fraction was obtained after red blood cell lysis with addition of ACK buffer (Biosource, Camarillo, CA). CD34+ cells were isolated using magnetic beads conjugated with anti-human CD34 (clone 561; Dynal, Lake Success, NY), which cross-reacts with cynomolgus CD34 [13]. The purity of CD34+ cells at harvest ranged from 90% to 95%, as assessed with another anti-human CD34 (clone 563; PharMingen, San Diego) that cross-reacts with cynomolgus CD34 [13]. The purity remained at the same levels after the 1-day transduction culture, which is discussed next.

Lentiviral Transduction

A simian immunodeficiency virus (SIV)-based lentivirus vector carrying enhanced jellyfish green fluorescent protein (GFP) (Clontech, Palo Alto, CA) was used for transduction. The vector was prepared as previously reported [14, 15]. All recombinant DNA experiments were approved by the Ministry of Education, Culture, Sports, Science and Technology of Japan.

CD34+ cells (1×10^6) were seeded in six-well plates in 2 ml of StemSpan serum-free expansion medium (Stem Cell Technologies, Vancouver) supplemented with recombinant human thrombopoietin (100 ng/ml; Kirin, Tokyo), recombinant human stem cell factor (100 ng/ml; Biosource, Camarillo, CA), recombinant human Flt-3 ligand (100 ng/ml; Research Diagnostics, Flanders, NJ), and antibiotics (100 U/ml of penicillin and 0.1 μg/ml of streptomycin; Meiji, Tokyo). The cells were transduced twice each for 12 hours (total, 24 hours) with the SIV vector at 50 transducing units per target cell. After transduction, cells were cryopreserved with 10% dimethylsulfoxide (Wako, Osaka, Japan) and 1% Dextran 40 (Yoshitomi, Osaka, Japan) in a controlled-rate programmable freezer (Kryo 10; Planer Biomed, Middlesex, UK) until transplantation. The viability of cells after thawing was 53.0 ± 6.5%, as assessed by trypan blue staining. An aliquot of transduced cells was assessed for GFP expression at 48 hours after transduction by flow cytometry using a FACScan (Becton Dickinson, Franklin Lakes, NJ) with excitation at 488 nm and fluorescence detection at 530 ± 30 nm.

In Vitro Endothelial Differentiation

CD34+ cells were seeded on fibronectin-coated plates (Becton Dickinson) in M199 medium (Invitrogen, Carlsbad, CA) with 20% fetal calf serum and bovine pituitary extracts (Invitrogen) as previously described [7]. After 7 days in culture, cells were examined for the uptake of DiI-acetylated low-density lipoprotein (LDL) and for the expression of CD31, von Willebrand factor (vWF), vascular endothelial (VE)-cadherin, and vascular endothelial growth factor receptor (VEGFR)-2. Briefly, adherent cells were incubated with 1 μg/ml of DiI-acetylated LDL (Molecular Probes, Eugene, OR) for 4 hours at 37°C. For immunofluorescence staining, after fixation in ice-cold 4% paraformaldehyde for 10 minutes and blocking in 1% bovine serum albumin (BSA) for 15 minutes, cells were incubated with a primary antibody: mouse anti-human CD31 (VM-59; Becton Dickinson), rabbit anti-human vWF (DakoCytomation, Glostrup, Denmark), mouse anti-human VE-cadherin (55-7H1; Becton Dickinson), or rabbit anti-mouse VEGFR2 (Santa Cruz Biotechnology, Santa Cruz, CA) for 1 hour at room

temperature. Cells were then incubated with a secondary antibody, Texas red–conjugated horse anti-mouse immunoglobulin G (IgG) (Vector, Burlingame, CA) or goat anti-rabbit IgG (Vector) for 30 minutes at room temperature.

Myocardial Infarction and Transplantation

All operations on cynomolgus monkeys were performed under an isoflurane-induced general anesthesia. Thoracotomy was conducted, the pericardium was opened, and the left anterior descending coronary artery was ligated with 5-0 prolene sutures. One to 2 hours after the ligation, GFP-transduced, autologous $CD34^+$ cells in normal saline were injected with a microsyringe through a 27-gauge needle into 10 sites (5 μl/site) in the peri-ischemic zone. In the control group, saline alone was injected in the same way. The pericardium and chest were closed. The animals then received butorphanol tartrate (0.5 mg/kg, intramuscularly) daily for 5 days to alleviate the pain associated with the operation and myocardial infarction.

Echocardiography

Echocardiographic imaging was obtained using a Sonos 5500 system (Philips Medical Systems, Andover, MA) before transplantation and at 2 weeks after transplant. The echocardiography was conducted by independent technicians irrelevant to our study group. In one animal (BM97080), it was additionally performed at 12 weeks. Short-axis two-dimensional images at the midpapillary level of the left ventricle were stored, and percent fractional shortening (%FS) was calculated to assess cardiac function.

Myocardial contrast echocardiography (MCE) was performed at day 0 (just before transplantation) and at 2 weeks after transplant to assess regional blood flow and blood flow defect size. In one animal (BM97080), chronic assessment was performed at 12 weeks after transplant. The electrocardiograph-triggered end-systolic intermittent imaging was conducted in short-axis views at incremental pulsing intervals (triggering intervals of 1, 2, 3, 4, and 8 beats) using an S12 probe. Once optimized, the settings of depth (4 cm), mechanical index (0.9), and focus (3 cm) were fixed. The contrast agent (perflutren; Yamanouchi, Tokyo) consisted of lipid-coated microbubbles of perfluorocarbon [16]. Perflutren diluted with saline (1:10) was administered intravenously at a constant rate (0.01 ml/kg per min). For the assessment of regional blood flow, MCE images were analyzed using ORIGIN 6.0J (Lightstone, Tokyo), and the blood flow was calculated as previously described [17]. Data are presented as a blood flow ratio (the peri-infarct versus nonischemic control region or the infarct versus nonischemic control region). For the assessment of blood flow defect, MCE images obtained at triggering interval of four beats were analyzed using National Institutes of Health Image software (version 1.61). Data are presented as percent defect compared with the total blood flow.

Microspheres

Colored microspheres (15 μm ± 2% diameter; E-Z Trac, Los Angeles) were used to evaluate regional blood flow 2 weeks after transplant [18], with the exception of one animal (BM97080), in which evaluation was performed 12 weeks after transplant. A set of microspheres (2×10^6) was diluted in 2 ml of saline and injected into the left ventricle over 30 seconds. A reference blood sample was withdrawn at a constant rate of 5 ml/min through the femoral artery. After the collection of blood samples, monkeys were irrigated with saline for mercy killing and blood was completely washed out. The heart was excised from each monkey. Tissue samples from the infarct, peri-infarct, and nonischemic regions (one sample per region) were digested, microspheres were collected, and the blood flow was calculated according to the manufacturer's instructions. Data are presented as blood flow ratio (the peri-infarct versus nonischemic control region or the infarct versus nonischemic control region).

Immunohistochemistry

Tissue samples from the infarct, peri-infarct, and nonischemic regions at 2 weeks after transplant were embedded in optimal cutting temperature compound (Sakura, Zoeterwoude, Netherlands) and frozen in liquid nitrogen. Sections were prepared (6 μm), fixed for 10 minutes at 4°C in 4% paraformaldehyde in phosphate-buffered saline (PBS), and blocked with 1% BSA in PBS. The sections were incubated at room temperature with a primary antibody, monoclonal mouse anti-human CD31 (1:200; Becton Dickinson), followed by a secondary antibody, biotin-conjugated horse anti-mouse IgG (1:500; Vector). The sections were then treated with avidin-alkaline phosphatase (ABC AP kit; Vector) for 30 minutes. The reaction was developed with a Vector Red substrate kit (SK-5100; Vector). In the case of double staining of CD31 and GFP, the above sections were further incubated with polyclonal rabbit anti-GFP (1:200; Clontech) followed by biotin-conjugated anti-rabbit IgG (1:500; Vector) and treated with avidin-peroxidase (ABC Elite kit; Vector). The reaction was developed with a Vector SG substrate kit (SK-4700; Vector). The sections were counterstained with hematoxylin, mounted in glycerol, and examined under a light microscope.

In Situ Polymerase Chain Reaction

In situ detection of transduced cell progeny was performed by amplifying proviral sequences as previously reported [19]. The following primer set for the GFP gene was used:

5'-CGT CCA GGA GCG CAC CAT CTT C-3' and 5'-GGT CTT TGC TCA GGG CGG ACT-3'. The polymerase chain reaction (PCR) mixture consisted of 420 μM dATP, 420 μM dCTP, 420 μM dGTP, 378 μM dTTP, 42 μM digoxigenin-labeled dUTP (Roche, Mannheim, Germany), 0.8 μM of each GFP primer, 4.5 mM $MgCl_2$, 1 × PCR buffer (Mg^{2+} free), and 4 U of Takara Taq DNA polymerase (Takara, Kyote). Sections were prepared with a Takara slide frame (Takara) from the infarct, peri-infarct, and nonischemic regions at 2 weeks after transplant. PCR was performed using a PTC100 thermal cycler (MJ Research, Watertown, MA) with the following conditions: 94°C for 1 minute and 57°C for 1 minute with 10 cycles. The digoxigenin-incorporated DNA fragments were detected using horseradish peroxidase (HRP)-conjugated rabbit F(ab') anti-digoxigenin antibody (DakoCytomation). The sections were then stained for HRP using a Vector SG substrate kit (Vector). Finally, the sections were counterstained with a Kernechtrot solution (Muto, Tokyo) that stains nucleotides, mounted in glycerol, and examined under a light microscope.

ELISA

Vascular endothelial growth factor (VEGF) and basic fibroblast growth factor (bFGF) levels in tissue lysate or medium were assessed by ELISA (R&D Systems, Minneapolis) according to the manufacturer's instructions. Tissue lysate was obtained from the peri-infarct region (three samples from each monkey) at 2 weeks after transplant. Briefly, tissue was homogenized and suspended in lysis buffer containing 10 mM Tris-HCl (pH 8.0), 1% Nonidet P-40, 150 mM NaCl, and protease inhibitor cocktail tablets (Complete Mini, Roche). The suspension was rocked at 4°C for 20 minutes and centrifuged at 16,000g and 4°C for 30 minutes. The supernatant was used for ELISA. The protein concentration of lysate was determined with DC Protein Assay (Bio-Rad, Hercules, CA).

Results

Lentiviral Marking

The CD34+ fraction of autologous bone marrow cells was used for transplantation in our study (Table 1). Before transplantation, CD34+ cells were genetically marked with GFP using an SIV-based lentivirus vector. The ex vivo transduction results are summarized in Table 1. The transduced cells were frozen until transplantation. An aliquot of the transduced cells was examined in vitro for the endothelial differentiation ability. After the differentiation culture, a vessel-like structure was observed (Fig. 1A). The ability of cells to take up DiI-acetylated LDL and the expression of CD31, vWF, VE-cadherin, and VEGFR-2 suggested the endothelial lineage (Fig. 1B). We and others have already confirmed the ability of hematopoietic differentiation of the cells [20, 21]. Taken together, the SIV-mediated GFP gene transfer does not spoil the differentiation abilities of CD34+ cells. In addition, on average, 41% of cells fluoresced 48 hours after transduction, and 56% of

Table 1. Summary of ex vivo transduction and transplantation

	Sex	Age (y)	Body weight (kg)	Harvested bone marrow cell number	Isolated CD34+ cell number	Transplanted cell number	% GFP expression Before[a]	% GFP expression After[b]
Saline group								
CTR01061[c]	M	3	4.1			NA		
CTR99056	M	3	3.4					
CTR96116	F	5	3.2					
CTR99051	M	5	5.9					
CD34+ cell group								
BM01052	M	3	3.9	213×10^6	1.00×10^6	0.47×10^6	49	87
BM01051[d]	M	3	4.1	396×10^6	5.14×10^6	2.20×10^6	51	54
BM97080[e]	M	5	3.9	330×10^6	2.35×10^6	1.04×10^6	49	67
BM90047	M	13	5.8	343×10^6	3.10×10^6	1.07×10^6	16	14
Average		5	4.3	321×10^6	2.90×10^6	1.20×10^6	41	56

[a]Before endothelial differentiation of GFP-transduced CD34+ cells.
[b]After the in vitro endothelial differentiation.
[c]CTR01061 died of heart failure 5 days after myocardial infarction.
[d]BM01051 developed a ventricular aneurysm after myocardial infarction.
[e]BM97080 was killed 12 weeks after the treatment. All other animals were killed 2 weeks after the treatment.
Abbreviations: GFP, green fluorescent protein; NA, not applicable.

endothelial cells still fluoresced after in vitro differentiation (Table 1), showing that the GFP expression is stable during the in vitro differentiation to endothelial cells. Thus, GFP was expected to serve as a good genetic tag after transplantation.

Acute Myocardial Infarction and Autologous Transplantation

Cynomolgus acute myocardial infarction was generated by ligating the left anterior descending artery. One to two hours after the ligation, GFP-transduced, autologous CD34$^+$ cells were injected in the peri-ischemic zone at 10 sites (total, $1.20 \pm 0.73 \times 10^6$ cells; $n = 4$). In the control group, saline was injected in the same way ($n = 4$). We conducted contrast echocardiography immediately after the coronary ligation and found no significant differences in the blood flow defect size (percent blood flow defect compared with the total) between the cell-treated and saline-treated groups ($13.0 \pm 2.1\%$ versus $12.3 \pm 3.5\%$, $p = .75$), suggesting that the initial risk of infarction did not differ between the two groups. In addition, we tried to assess the cardiac isozyme of serum creatine kinase (CK) to evaluate the infarct size; however, either the immuno-inhibition assay or chemical luminescence immunoassay did not work well for cynomolgus monkey samples. We were at least able to show that total CK values at 24 hours after the ligation did not significantly differ between the two groups ($p = .83$).

One of the control monkeys (CTR01061) died of heart failure 5 days after myocardial infarction, and the other control monkeys showed a decrease in %FS at 2 weeks after infarction (Fig. 2). Thus, all four control animals showed the deteriorated cardiac function. In the cell-treated group, one monkey (*, BM01051) underwent ventricular fibrillation immediately after the ligation and survived after cardiopulmonary resuscitation but eventually developed a ventricular aneurysm. Only this animal showed a decrease in %FS despite CD34$^+$ cell treatment; the other animals receiving CD34$^+$ cells showed an increase in %FS (Fig. 2). CD34$^+$ cell treatment may not be able to rescue such a heavily impaired heart but otherwise had a significant effect on cardiac function. Even an old monkey (BM90047, Table 1) showed improved %FS.

The relative blood flow in the peri-infarct to nonischemic control region was also significantly ameliorated in the CD34$^+$ cell–treated monkeys compared with the saline-treated ones, as assessed using contrast echocardiography (Fig. 3A) and colored microspheres (Fig. 3B). An excellent correlation was found between the two methods (Fig. 3C; correlation coefficient = 0.93). Two groups (CD34$^+$ cell–treated and saline-treated) were well separated on the panel, showing an obvious positive effect of CD34$^+$ cell injection on the blood flow in the peri-infarct zone after acute myocardial infarction. In fact, the average myocardial blood flow in the peri-infarct region in the absolute value was 0.988 ml/g per minute and 0.383 ml/g per minute for the cell-treated and saline-treated groups, respectively. Of note, the blood flow in the peri-infarct zone was ameliorated even in the animal with a ventricular aneurysm. On the other hand, the relative blood flow in the infarct to nonischemic region did not show

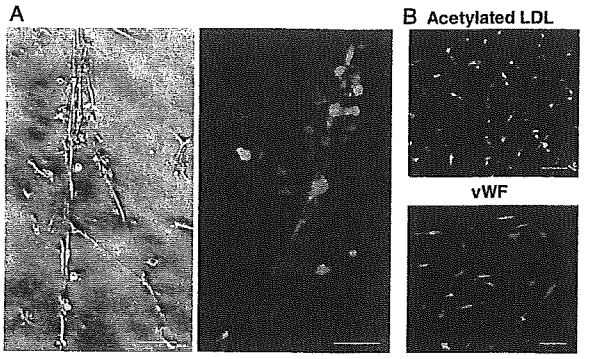

Figure 1. In vitro endothelial differentiation of cynomolgus CD34$^+$ cells lentivirally transduced with GFP. The transduced CD34$^+$ cells were differentiated to endothelial cells after 7 days in culture. **(A)**: Representative vessel-like structure derived from CD34$^+$ cells observed under a phase-contrast microscope (left) and a fluorescent microscope (right). **(B)**: The transduced CD34$^+$ cells differentiated into fluorescent cells (green) positive for the cellular intake of acetylated LDL and immunostaining for von Willebrand factor (vWF) (stained in red). Bar = 100 μm. Abbreviations: GFP, green fluorescent protein; LDL, low-density lipoprotein.

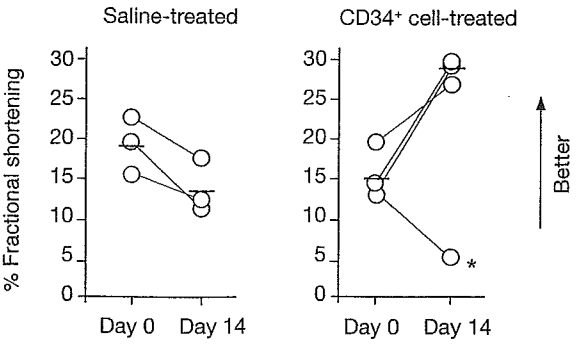

Figure 2. Improved cardiac function after CD34$^+$ cell transplantation. Cardiac function was assessed by echocardiography in terms of percent fractional shortening (%FS) before and 2 weeks after treatment. One monkey in the saline-treated group (CTR01061) died of heart failure 5 days after myocardial infarction and is not included in the figure. One monkey in the CD34$^+$ cell–treated group (*, BM01051) developed a left ventricular aneurysm after myocardial infarction. If this animal was excluded from the statistical analysis, the cardiac function was significantly improved in the CD34$^+$ cell–treated compared with the saline-treated group in terms of the ratio of %FS at day 14 versus day 0 after transplant ($p = .017$).

a significant difference between the CD34+ cell–treated and saline-treated groups. The peri-infarct region was the injection site, and thus the highest degree of change would be expected there.

All monkeys except one CD34+ cell–treated monkey (BM97080) were examined for cardiac function and blood flow at 2 weeks after transplantation, and their tissue sections were finally prepared at this time point (see below). BM97080 was examined at 12 weeks, at which time the cardiac function was still improved compared with immediately after infarction (data not shown) and the blood flow data were in a position similar to the cell-treated group at 2 weeks (Fig. 3C).

In Vivo Tracking of Transplanted Cells

Two weeks after the transplantation, tissue sections were prepared from the infarct, peri-infarct, and nonischemic regions. Immunostaining of an endothelial marker CD31 demonstrated more vessels in the peri-infarct region of the CD34+ cell-treated than saline-treated myocardium (Fig. 4A). In fact, the capillary density of the peri-infarct region was significantly better preserved in the cell-treated than saline-treated group, although there was no significant difference in the capillary density of the nonischemic control regions between the two groups (Fig. 4B).

Double immunostaining with anti-CD31 and anti-GFP showed that some cells in vessels were positive for both CD31 and GFP in the peri-infarct region (Fig. 5A). The result clearly indicates that at least some transplanted CD34+ cells gave rise to endothelial cells. However, we found that the transplanted cell progeny accounted for only a small fraction of endothelial cells after examining more than 100 sections of the peri-infarct region. In situ PCR for proviral GFP sequences also showed that few CD31-positive endothelial cells contained the GFP-provirus (Fig. 5B). There were no GFP-positive cardiomyocytes in more than 100 sections. Most of the transplanted cell progeny were found not incorporated in vessels (Fig. 5C). Hematoxylin-eosin staining did not show any noncardiac tissue regeneration in the myocardium.

On the other hand, we found that in vitro conditioned medium of CD34+ cell culture for endothelial differentiation contained high levels of VEGF, whereas unconditioned medium did not contain detectable VEGF, as assessed

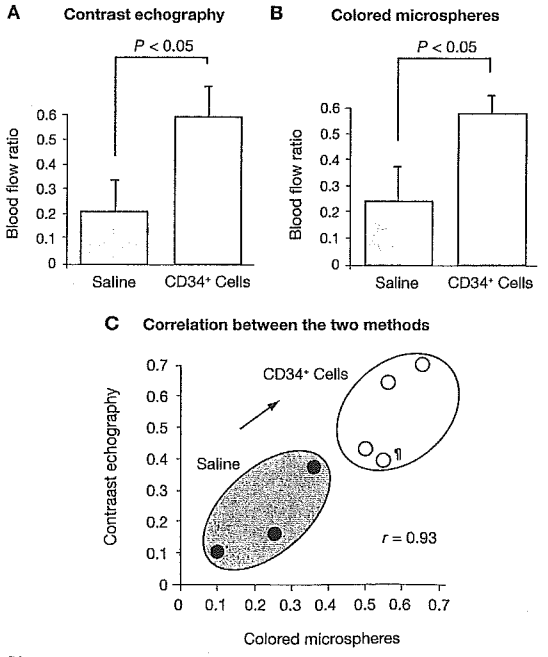

Figure 3. Improved regional blood flow after CD34+ cell transplantation. Myocardial contrast echocardiography (**A**) and colored microspheres (**B**) showed a significantly ameliorated blood flow ratio (the peri-infarct to nonischemic control region) in the CD34+ cell–treated monkeys ($n = 3$) compared with the saline-treated monkeys ($n = 3$) at 2 weeks after treatment. (**C**): An excellent correlation was found between the two methods. A CD34+ cell–treated monkey (¶, BM97080) that was examined at 12 weeks after transplant is included in the panel (**C**) but excluded from the statistical analysis in (**A**) and (**B**).

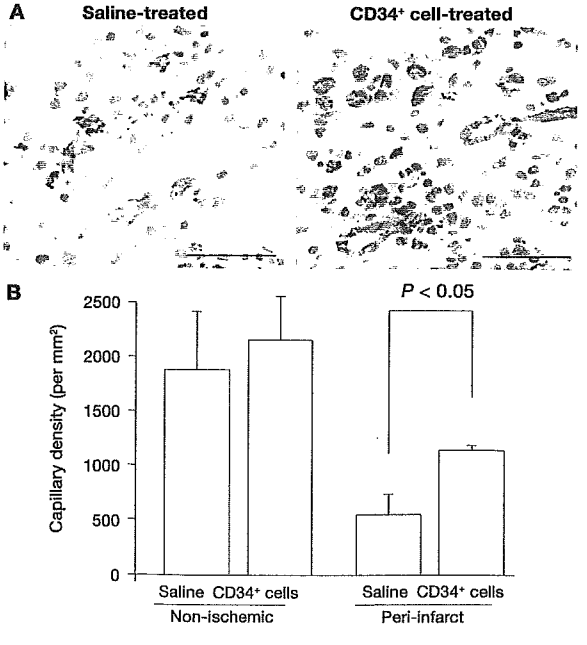

Figure 4. Neoangiogenesis in the ischemic myocardium. Tissue sections were prepared at 2 weeks after the treatment. (**A**): Representative results of immunostaining with anti-CD31 (stained in brown) in the peri-infarct region of the saline-treated and CD34+ cell–treated myocardium. Bar = 50 μm. (**B**): The density of CD31-positive capillaries in the peri-infarct and control nonischemic regions in the saline-treated and CD34+ cell–treated groups. Five fields for each section were randomly selected ($n = 3$ for the saline injection, $n = 3$ for the CD34+ cell injection), and the number of CD31-positive capillaries was counted (average ± standard deviation).

by ELISA (Fig. 6A). In addition, in vivo VEGF levels in the peri-infarct tissue were significantly higher in the CD34$^+$ cell–treated than saline-treated group (Fig. 6B, left), although in vivo levels of bFGF differed little between the two groups (Fig. 6B, right).

Discussion

Although gained with small numbers of cynomolgus monkeys, our data suggest that the direct transplantation of bone marrow CD34$^+$ cells, even without coronary bypass grafts or percutaneous coronary intervention, results in improved regional blood flow and cardiac function after myocardial infarction in nonhuman primates. Furthermore, we have tried to see the contribution of transplanted CD34$^+$ cells to the repair of ischemic myocardium. To this end, we genetically marked CD34$^+$ cells with GFP using an SIV-based lentiviral vector before transplantation. Lentiviral vectors can transduce nondividing cells unlike oncoretroviral vectors, and thus the ex vivo culture period with multiple cytokines to allow cell cycling can be reduced to 1 day or less [20, 22, 23]. This is the great advantage of using lentiviral vectors over oncoretroviral vectors for transduction of multipotent stem cells, given that extended ex vivo culture of stem cells may result in loss of multilineage differentiation and engraftment abilities [24]. Human immunodeficiency virus (HIV)-1–based lentiviral vectors can efficiently transduce human cells, but not Old World monkey cells [25]. According to a recent report, a species-specific cytoplasmic component confers the innate

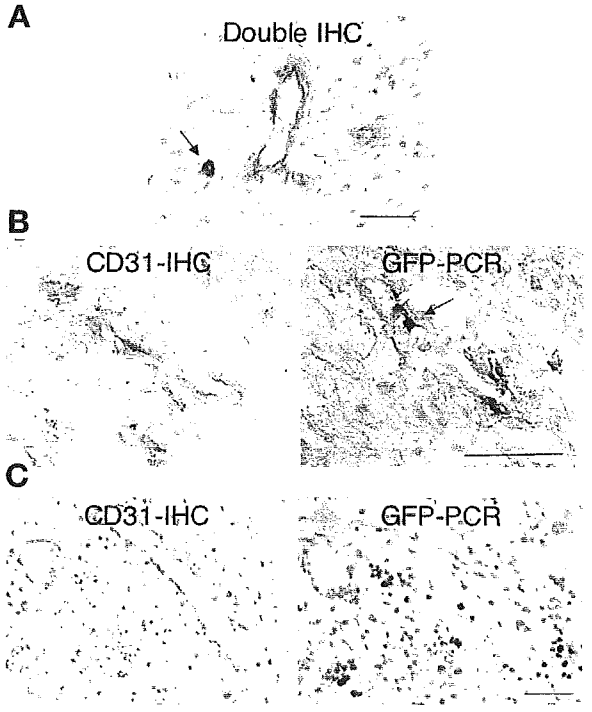

Figure 5. In vivo fate of transplanted cells. Cardiac sections were prepared at 2 weeks after transplantation. **(A)**: Double immunohistochemistry (IHC) with anti-CD31 and anti–green fluorescent protein (GFP) in the peri-infarct region of the CD34$^+$ cell–treated myocardium. Some cells (arrow) were positive for both CD31 (stained in brown) and GFP (stained in black), but such cells were rare. **(B, C)**: Serial sections from the peri-infarct region of the CD34$^+$ cell–treated myocardium. One section (left) was stained with anti-CD31 (stained in brown), and the other (right) was assessed by in situ polymerase chain reaction (PCR) for proviral GFP sequences (stained in black). **(B)**: Some CD31-positive endothelial cells contained the GFP-provirus (arrow, right panel), but such cells were rare. **(C)**: Transplanted cell progeny (cells positive for GFP-provirus in the right panel) were not incorporated in vessels (cells positive for CD31 in the left panel). Bar = 50 μm.

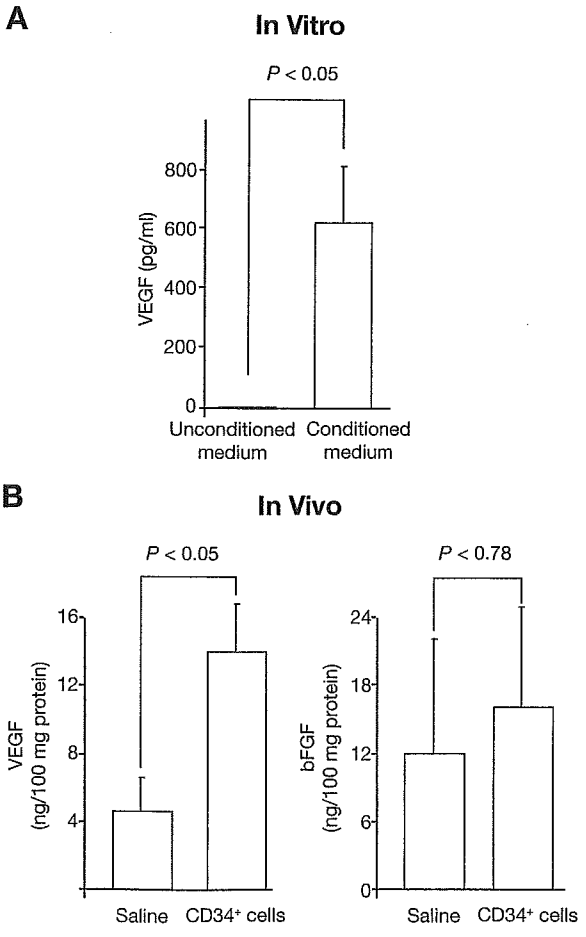

Figure 6. VEGF is implicated in the neoangiogenesis. **(A)**: Unconditioned and conditioned media of in vitro CD34$^+$ cell cultures for endothelial differentiation were examined for VEGF by ELISA. The average ± standard error of six culture dishes is shown. **(B)**: Lysates (three samples per monkey) from the peri-infarct region of the CD34$^+$ cell–treated (monkey, n = 3) and saline-treated (monkey, n = 3) myocardium were prepared and examined for VEGF and basic fibroblast growth factor (bFGF) by ELISA. Data are shown as the average ± standard error. Abbreviation: VEGF, vascular endothelial growth factor.

postentry restriction to HIV-1 infection in simian cells [26]. Unlike HIV-1–based lentiviral vectors, SIV-based ones can efficiently transduce simian hematopoietic stem/progenitor cells [21]. In this study, we also used an SIV-based lentiviral vector and achieved the efficient gene transfer into simian CD34+ cells.

As a result of this marking study, we found only a few GFP-positive cells incorporated into the vascular structure in the ischemic myocardium at 2 weeks after transplantation. GFP-positive cardiomyocytes were not detectable. The existence of GFP-positive endothelial cells can be explained by fusion events [27, 28]. However, if that is the case, GFP-positive cardiomyocytes should have also been detected, given that cardiomyocytes are even easier targets of fusion than endothelial cells [11, 29]. Whether fusion occurred or not, only a few transplanted cells gave rise to nonhematopoietic cells in our primate model.

There are several possible explanations for the very low prevalence of transplanted cell–derived endothelial cells or cardiomyocytes in the ischemic myocardium. First, 2 weeks was too short or the number of transplanted cells was too small to see the nonhematopoietic differentiation. However, the cardiac function and regional blood flow were ameliorated by this time point and with this number of transplanted cells. Thus, if transplanted cell–derived, nonhematopoietic differentiation was a reason for the improvement, transplanted cells at this number should have given rise to such cells by this time point. In fact, Orlic et al. [8] observed transplanted cell-derived endothelial cells and cardiomyocytes within 11 days after transplant in mice. In addition, we observed the endothelial differentiation from CD34+ cells within 7 days in vitro (Fig. 1). However, we cannot formally rule out a possibility that inflammatory responses after generation of infarction might have negative effects on engraftment of transplanted cells. Second, the SIV vector failed to transduce stem or progenitor cells that might be responsible for nonhematopoietic differentiation. Even if the transduction was successful, the cytokine treatment during the transduction or GFP expression in the cells spoiled the differentiation abilities. However, we have shown that the SIV vector successfully transduced cells that were capable of differentiating into GFP-expressing endothelial cells (Fig. 1). We have not examined the differentiation ability to cardiomyocytes, because the method to differentiate CD34+ cells to cardiomyocytes in vitro has not been well established. Thus, we cannot formally rule out the possibility that the ex vivo culture spoiled the ability to differentiate to cardiomyocytes or reduced the ability to differentiate to endothelial cells. Third, cells expressing xenogeneic GFP were rejected via immune responses. However, 2 weeks is too short to allow immune elimination of GFP-expressing cells in monkeys [30, 31]. Fourth, the GFP expression was shut down because of transcriptional silencing in vivo, resulting in negative immunostaining with anti-GFP. To examine this possibility, we tried to detect the provirus (vector integrated into genome) in the cardiac tissue by in situ PCR and found again that only a few CD31-positive endothelial cells contained the GFP-provirus (Fig. 5B), thus arguing against transcriptional silencing-based negative immunostaining with anti-GFP. Taken together, we concluded that most transplanted cell progeny were not incorporated into the repaired, nonhematopoietic tissues.

Our results are in agreement with recent reports that transplanted hematopoietic cells are unable to transdifferentiate into nonhematopoietic cells in ischemic myocardium in mice [9–11]. Our studies confirm and extend these findings in a couple of ways. First, we show that the cardiac function can be indeed significantly improved after injection of hematopoietic cells in a nonhuman primate model, although the above studies used murine myocardial infarction models and did not address the potential beneficial effects of hematopoietic cell injection. Second, the improvement is unlikely to be the result of generation of transplanted cell–derived endothelial cells or cardiomyocytes. Finally, we have found that cultured CD34+ cells secrete VEGF and that the CD34+ cell–treated myocardium contains a significantly higher level of VEGF than the saline-treated myocardium. This observation raises a possibility that some angiogenic cytokines secreted from transplanted cells (paracrine effects) potentiate angiogenic activity of endogenous cells. VEGF would be a candidate. Despite this, the delivery of a single agent (VEGF) failed in clinical trials for cardiac ischemia [32]. In situ multiple cytokine production and coordinated action may be essential for clinical benefits [33, 34]. It will be important to explore and identify cytokines responsible for the paracrine effect. If transplanted cells serve as cytokine factories rather than stem cells in ischemic tissues, it is not surprising that not only stem cells but other types of cells may also work [35]. The concept of stem cell therapeutics for ischemic diseases needs additional consideration.

Acknowledgments

The SIV vector was supplied by DNAVEC Corporation (Ibaraki, Japan), and thrombopoietin was supplied by Kirin Brewery Co. Ltd. (Tokyo). We thank Masahiro Shakudo (Sumiyoshi Hospital, Osaka) for analyzing the contrast echocardiography and Yasuhiro Ochiai (Jichi Medical School) for preparing tissue sections.

References

1 Assmus B, Schachinger V, Teupe C et al. Transplantation of progenitor cells and regeneration enhancement in acute myocardial infarction (TOPCARE-AMI). Circulation 2002;106:3009–3017.

2 Strauer BE, Brehm M, Zeus T et al. Repair of infarcted myocardium by autologous intracoronary mononuclear bone marrow cell transplantation in humans. Circulation 2002;106:1913–1918.

3 Tse HF, Kwong YL, Chan JK et al. Angiogenesis in ischaemic myocardium by intramyocardial autologous bone marrow mononuclear cell implantation. Lancet 2003;361:47–49.

4 Perin EC, Dohmann HF, Borojevic R et al. Transendocardial, autologous bone marrow cell transplantation for severe, chronic ischemic heart failure. Circulation 2003;107:2294–2302.

5 Stamm C, Westphal B, Kleine HD et al. Autologous bone-marrow stem-cell transplantation for myocardial regeneration. Lancet 2003;361:45–46.

6 Wollert KC, Meyer GP, Lotz J et al. Intracoronary autologous bone-marrow cell transfer after myocardial infarction: the BOOST randomised controlled clinical trial. Lancet 2004;364:141-148.

7 Asahara T, Murohara T, Sullivan A et al. Isolation of putative progenitor endothelial cells for angiogenesis. Science 1997;275:964–967.

8 Orlic D, Kajstura J, Chimenti S et al. Bone marrow cells regenerate infarcted myocardium. Nature 2001;410:701–705.

9 Murry CE, Soonpaa MH, Reinecke H et al. Haematopoietic stem cells do not transdifferentiate into cardiac myocytes in myocardial infarcts. Nature 2004;428:664–668.

10 Balsam LB, Wagers AJ, Christensen JL et al. Haematopoietic stem cells adopt mature haematopoietic fates in ischaemic myocardium. Nature 2004;428:668–673.

11 Nygren JM, Jovinge S, Breitbach M et al. Bone marrow-derived hematopoietic cells generate cardiomyocytes at a low frequency through cell fusion, but not transdifferentiation. Nat Med 2004;10:494–501.

12 Hanazono Y, Terao K, Ozawa K. Gene transfer into nonhuman primate hematopoietic stem cells: implications for gene therapy. STEM CELLS 2001;19:12–23.

13 Shibata H, Hanazono Y, Ageyama N et al. Collection and analysis of hematopoietic progenitor cells from cynomolgus macaques (Macaca fascicularis): assessment of cross-reacting monoclonal antibodies. Am J Primatol 2003;61:3–12.

14 Nakajima T, Nakamaru K, Ido E et al. Development of novel simian immunodeficiency virus vectors carrying a dual gene expression system. Hum Gene Ther 2000;11:1863–1874.

15 VandenDriessche T, Thorrez L, Naldini L et al. Lentiviral vectors containing the human immunodeficiency virus type-1 central polypurine tract can efficiently transduce nondividing hepatocytes and antigen-presenting cells in vivo. Blood 2002;100:813–822.

16 Kobayashi N, Yasu T, Yamada S et al. Influence of contrast ultrasonography with perflutren lipid microspheres on microvessel injury. Circ J 2003;67:630–636.

17 Wei K, Jayaweera AR, Firoozan S et al. Quantification of myocardial blood flow with ultrasound-induced destruction of microbubbles administered as a constant venous infusion. Circulation 1998;97:473–483.

18 Hale SL, Alker KJ, Kloner RA. Evaluation of nonradioactive, colored microspheres for measurement of regional myocardial blood flow in dogs. Circulation 1988;78:428–434.

19 Haase AT, Retzel EF, Staskus KA. Amplification and detection of lentiviral DNA inside cells. Proc Natl Acad Sci U S A 1990;87:4971–4975.

20 Hanazono Y, Asano T, Ueda Y et al. Genetic manipulation of primate embryonic and hematopoietic stem cells with simian lentivirus vectors. Trends Cardiovasc Med 2003;13:106–110.

21 Hanawa H, Hematti P, Keyvanfar K et al. Efficient gene transfer into rhesus repopulating hematopoietic stem cells using a simian immunodeficiency virus-based lentiviral vector system. Blood 2004;103:4062–4069.

22 Miyoshi H, Smith KA, Mosier DE et al. Transduction of human $CD34^+$ cells that mediate long-term engraftment of NOD/SCID mice by HIV vectors. Science 1999;283:682–686.

23 Horn PA, Keyser KA, Peterson LJ et al. Efficient lentiviral gene transfer to canine repopulating cells using an overnight transduction protocol. Blood 2004;103:3710–3716.

24 Dunbar CE, Takatoku M, Donahue RE. The impact of ex vivo cytokine stimulation on engraftment of primitive hematopoietic cells in a non-human primate model. Ann N Y Acad Sci 2001;938:236–245.

25 Owens CM, Yang PC, Gottlinger H et al. Human and simian immunodeficiency virus capsid proteins are major viral determinants of early, postentry replication blocks in simian cells. J Virol 2003;77:726–731.

26 Stremlau M, Owens CM, Perron MJ et al. The cytoplasmic body component TRIM5α restricts HIV-1 infection in Old World monkeys. Nature 2004;427:848–853.

27 Terada N, Hamazaki T, Oka M et al. Bone marrow cells adopt the phenotype of other cells by spontaneous cell fusion. Nature 2002;416:542–545.

28 Ying QL, Nichols J, Evans EP et al. Changing potency by spontaneous fusion. Nature 2002;416:545–548.

29 Alvarez-Dolado M, Pardal R, Garcia-Verdugo JM et al. Fusion of bone-marrow-derived cells with Purkinje neurons, cardiomyocytes and hepatocytes. Nature 2003;425:968–973.

30 Rosenzweig M, Connole M, Glickman R et al. Induction of cytotoxic T lymphocyte and antibody responses to

enhanced green fluorescent protein following transplantation of transduced CD34(+) hematopoietic cells. Blood 2001;97:1951–1959.

31 Heim DA, Hanazono Y, Giri N et al. Introduction of a xenogeneic gene via hematopoietic stem cells leads to specific tolerance in a rhesus monkey model. Mol Ther 2000;1:533–544.

32 Henry TD, Annex BH, McKendall GR et al. The VIVA trial: vascular endothelial growth factor in ischemia for vascular angiogenesis. Circulation 2003;107:1359–1365.

33 Cao R, Brakenhielm E, Pawliuk R et al. Angiogenic synergism, vascular stability and improvement of hind-limb ischemia by a combination of PDGF-BB and FGF-2. Nat Med 2003;9:604–613.

34 Ziegelhoeffer T, Fernandez B, Kostin S et al. Bone marrow-derived cells do not incorporate into the adult growing vasculature. Circ Res 2004;94:230–238.

35 Kinnaird T, Stabile E, Burnett MS et al. Local delivery of marrow-derived stromal cells augments collateral perfusion through paracrine mechanisms. Circulation 2004;109:1543–1549.

Available online at www.sciencedirect.com
SCIENCE DIRECT
Microbes and Infection 7 (2005) 126–131
Microbes and Infection
www.elsevier.com/locate/micinf

Original article

Isolation and characterization of a new simian retrovirus type D subtype from monkeys at the Tsukuba Primate Center, Japan

Masayuki Hara [a,b], Tetsutaro Sata [c], Toshihiko Kikuchi [a], Noriko Nakajima [c], Akihiko Uda [a], Koji Fujimoto [d], Tadashi Baba [b], Ryozaburo Mukai [a,*]

[a] *Tsukuba Primate Center for Medical Science, National Institute Infectious Diseases (NIID), 1 Hachimanndai, Tsukuba 305-0843, Japan*
[b] *Graduate School of Life and Environmental Sciences, Institute of Applied Biochemistry, University of Tsukuba, 1-1-1 Tennodai, Tsukuba 305-8572, Japan*
[c] *Department of Infectious Pathology, National Institute of Infectious Diseases, Tokyo 162-8640, Japan*
[d] *The Corporation for Production and Research of Laboratory Primates, 1 Hachimanndai, Tsukuba 305-0843, Japan*

Received 15 June 2004; accepted 30 August 2004

Available online 10 December 2004

Abstract

Exogenous type D simian retroviruses (SRV/D) are prevalent in captive and feral populations of various macaque monkeys. Thus far, five subtypes of SRV/Ds have been reported, three of which (SRV-1, -2 and -3) have been molecularly characterized. Two SRV/D strains (N27 and T150) were isolated from seropositive cynomolgus macaques at the Tsukuba Primate Center (TPC) in Japan, showing clinical signs of SRV/D infection, including anemia and persistent unresponsive diarrhea. Electron microscopy demonstrated that both SRV/D isolates have a virion morphology typical of type D retrovirus. The SRV/D N27 and T150 isolates were essentially the same based on sequence analysis. From homology analysis of the entire *gag* sequence, the N27 isolate is closely related to the other known SRV/Ds but is distinct from the three molecularly characterized SRV/Ds. Thus, we have tentatively designated the N27 and T150 viruses isolated from TPC cynomolgus macaques as SRV/D-Tsukuba (SRV/D-T).
© 2004 Elsevier SAS. All rights reserved.

Keywords: Simian retrovirus type D; Cynomolgus macaque; Virus isolation; *gag* sequence

1. Introduction

Infection with simian retrovirus type D (SRV/D) is prevalent in wild as well as colony-born macaques [1–3]. Different isolates are associated with different macaque species at different primate research centers [2]. Thus far, five subtypes have been identified based on virus neutralization [2–5], of which three (SRV-1, SRV-2, and Mason–Pfizer monkey virus; MPMV; SRV-3) have been molecularly cloned and sequenced [6–8]. SRV-4 was isolated from a cynomolgus macaque at University of California, Davis, but its molecular characterization has not been reported. Recently, the partial *gag-prt* sequence of SRV-5 was determined [9]. Also, SRV/D-6 was isolated from a Hanuman langur and its partial sequence was reported [10,11].

SRV/D has been identified as one of the causes of simian acquired immunodeficiency syndrome (SAIDS), a naturally occurring immunosuppressive and sometimes fatal disease of macaques. Animals suffering from advanced SAIDS may exhibit lymphadenopathy, splenomegaly, anemia, lymphoid depletion, bone marrow hyperplasia, weight loss, persistent unresponsive diarrhea, chronic opportunistic infections and malignant neoplasia [12].

Macaques are needed for a variety of biomedical studies such as preclinical studies and/or safety testing of vectors for gene therapy in which immunosuppressive treatments may result in an increase in the viral load of SRV/D. Also, macaque models provide an opportunity to develop vaccines against simian immunodeficiency virus (SIV), which induces a disease similar to human AIDS. Thus, the detection and eradi-

Abbreviations: CPE, cytopathic effect; PBMCs, peripheral blood mononuclear cells; SAIDS, simian acquired immunodeficiency syndrome; SRV/D, simian retrovirus type D; TPC, Tsukuba Primate Center.

* Corresponding author. Tel.: +81-298-37-2121; fax: +81-298-37-0218.
E-mail address: mukai@nih.go.jp (R. Mukai).

1286-4579/$ - see front matter © 2004 Elsevier SAS. All rights reserved.
doi:10.1016/j.micinf.2004.08.021

cation of SRV/D infection in macaque breeding colonies is of great importance.

The prevalence of SRV/D infections in the cynomolgus macaque breeding colony at Tsukuba Primate Center (TPC) has been estimated by serological testing. However, whether the monkeys are really infected with SRV/D or not and the subtype of the SRV/D, if any, are not known. In this study, we report the results of analysis of SRV/D viruses isolated from two seropositive cynomolgus monkeys at TPC that exhibited the characteristic clinical signs of SRV/D infection.

2. Materials and methods

2.1. Animals

The two female cynomolgus monkeys (*Macaca fascicularis*) described in this report (no. 27 and no. 150) were bred and reared at TPC, National Institute of Infectious Diseases. The familial lineages of these two monkeys were unrelated. Although serological testing at 6 months of age indicated that monkey no. 27 was positive for SRV/D; she exhibited normal weight gain and growth up to 2 years of age. At this time, body weight and red blood cell (RBC) counts decreased, respectively, from 1.90 to 1.68 kg and from 590 to 166×10^7 per ml in the next 6 months. When blood was collected for SRV/D virus isolation at 2.5 years of age, this monkey had occasional diarrhea. Although monkey no. 150 was known to be seropositive to SRV/D at 6 years of age, she remained apparently healthy until 7 years of age. Over a 3-month period, body weight decreased from 3.26 to 2.88 kg and she developed unresponsive diarrhea. RBC counts also decreased from 611 to 86×10^7 per ml during this period. At the time peripheral blood samples were collected from these monkeys for serology and virus isolation, both monkeys were positive for SRV/D by Western blotting analysis.

2.2. Virus isolation

Peripheral blood mononuclear cells (PBMCs) were isolated from monkeys no. 27 and no. 150 by Ficoll gradient centrifugation, washed in phosphate-buffered saline (PBS), and aliquoted at 10^6 cells per ml. Approximately 5×10^5 PBMCs were cocultured with 2×10^5 Raji cells (a Burkitt's lymphoma B-cell line) in complete medium which consisted of RPMI-1640 supplemented with 10% fetal calf serum, 2-mercapto-ethanol (50 μM), sodium pyruvate (1 mM), penicillin (100 IU/ml), streptomycin (100 μg/ml), concanavalin A (10 μg/ml), and recombinant interleukin-2 (200 U/ml) (Shionogi and Co., Ltd., Osaka, Japan). Viral cytopathic effect (CPE) and reverse transcriptase (RT) activity were monitored during co-cultivation.

2.3. Electron microscopic analysis

When CPE became widespread in Raji cells co-cultivated with PBMCs from a monkey No. 27, cells were fixed in ice-cold 2.5% glutaraldehyde in 0.1 M sodium cacodylate buffer (pH 7.5) and washed with 0.1 M cacodylate buffer containing 0.1 M sucrose. The fixed cells were embedded in Epon 812 resin and ultra-thin sections were prepared, stained with lead citrate/uranium acetate, and analyzed by electron microscope (Hitachi H7600).

2.4. Western blotting

Antibodies to SRV/D were screened by Western blotting using SRV/D-2 antigen supplied by Bio-Reliance (MD, USA). The criterion for a positive reaction was detection of two or more virion-specific bands (i.e. gag and env).

2.5. Polymerase chain reaction

DNA from SRV/D-infected Raji cells was extracted using NucleoSpin Blood Kit (MACHEREY-NAGEL, Duren, Germany). The *gag* region (222 bp) was amplified by nested PCR using primers that detect SRV/D-1, -2, and -3 (WH1, WH3 and RC12–15) [13]. Other *gag* primer sets (p27F1, p27R1 and p27F2, p27R2) that detect part of the p27 region of SRV/D-1 to -5 were also used [14].

The entire *gag* region was amplified by PCR using primers gast4, 5′-AGCGAAAGTACATTGTCTTA-3′ and RR111, 5′-TCATTGTCGACAACCCCTGGA-3′. PCR was performed with 500 ng of genomic DNA, 20 pmol of each primer, 10 mM Tris–HCl (pH 8.0), 50 mM KCl, 2.5 mM $MgCl_2$, 0.4 mM dNTPs and 2.5 units of Takara LA *Taq* polymerase (Takara, Ohtsu, Japan) in a total volume of 50 μl. PCR was performed in a Peltier Thermal Cycler Model PTC-200 (MJ Research, Tokyo, Japan). Amplification was performed as follows: one cycle at 95 °C for 4 min; 30 cycles at 94 °C for 1 min; 54 °C for 1 min and 72 °C for 4 min; and one cycle at 72 °C for 10 min. Amplified PCR products were visualized by electrophoresis in 0.5% agarose gels stained with 0.5 mg/ml ethidium bromide under ultraviolet transillumination.

2.6. DNA sequencing

PCR products were purified using an Ultra Clean GelSpin Kit (MO BIO, CA, USA) and were directly sequenced using the BigDye Terminator Ver. 1.1 Cycle sequencing Kit (Applied Biosystems, Tokyo, Japan), according to the manufacturer's protocol. The templates were subjected to one cycle at 96 °C for 1 min, 25 cycles at 96 °C for 10 s, 50 °C for 5 s and 60 °C for 4 min. Electrophoresis was performed on an ABI PRISM 3100-Avant Genetic Analyzer (Applied Biosystems).

2.7. Analysis and alignment of nuculeotide sequences and amino acid sequences

Analysis and alignment of nuculeotide sequences and amino acid sequences were done with GENETYX Ver. 10.1.4

(genetyx@SDC.co.jp). Gaps introduced for optimal alignment were not considered informative and were not included in the analyses. Distances were estimated by Kimura's two-parameter method for nucleotide substitution [15]. The phylogenetic trees were constructed by the neighbor-joining (NJ) method [16]. The GenBank accession numbers of the sequences used for comparison were SRV/D-1 (M11841) [6], SRV/D-2 (AF126467) [17], SRV/D-3 (M12349) [7], BaEV (D10032) [18], SMRV-H (M23385) [19], GALV (M26927) [20], SFV (X54482) [21], HTLV-1 (L03561) [22], HTLV-2 (NC-001488) [23], STLV-2 (NC-001815) [24] and RSV (J02342) [25]. The *gag* sequence from the strain SRV/D N27 (SRV/D-Tsukuba, SRV/D-T) has been deposited in GenBank (DDBJ) under accession number AB181392.

3. Results

3.1. Isolation of SRV/D from cynomolgus monkeys

When PBMCs of the two monkeys that developed SAIDS with SRV/D were co-cultivated with Raji cells, typical SRV/D CPE including syncytia was observed after 4 days (Fig. 1A). RT activity was also detected in the culture supernatant, and Raji cells with syncytia were positive by indirect immunofluorescent antibody assay using anti-SRV/D-2 serum. When these infected Raji cells were subjected to electron microscopic analysis, typical A-particle-like virions (90 nm in diameter) were observed in the cytoplasm and mature type D particles (120 nm in diameter) were observed outside of the cells (Figs. 1C,D) [4]. SRV/Ds isolated from monkeys No. 27 and No. 150 were tentatively designated SRV/D N27 and SRV/D T150, respectively.

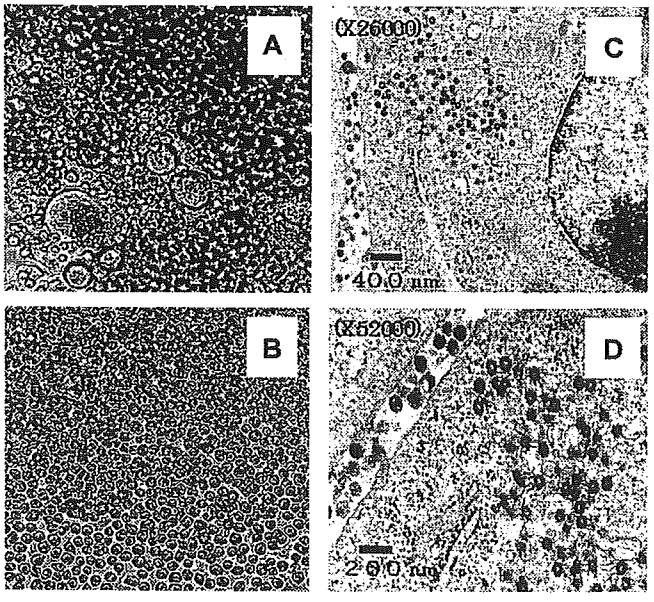

Fig. 1. CPE and virion morphology of Raji cells infected with SRV/D isolate from cynomolgus monkey No. 27. A: Infected Raji cells with large syncytia (×100). B: Uninfected Raji cells (×100). C: Electron micrograph of infected Raji cells (×26,000). D: Higher magnification electron micrograph of cytoplasmic 90-nm type A retrovirus particles and extracellular mature type D retroviruses.

3.2. Characterization of isolated SRV/D from TPC

The genomic DNA from Raji cells infected with the N27 and T150 isolates were subjected to PCR analysis to amplify the *gag* region, using primer sets (WH1, WH3 and RC12–15) which detect only SRV/D-1, -2 and -3 [13]. These primers give a strong signal for these three viruses at both the first and second rounds of the nested PCR, but not for SRV/D-4 or -5 (N.W. Lerche, California National Primate Research Center, USA, personal communication). No amplified band was observed at the first amplification using WH1, WH3 primer sets on the genomic DNA of Raji cells infected with the N27 or T150 isolates. However, a 232-bp band was detected by nested PCR with the RC12–15 primers (data not shown). Furthermore, a 461-bp and a 400-bp band were observed on first and second rounds of PCR, respectively, using published primer sets (p27F1, p27R1 and p27F2, p27R2) [14]. These primers detect the p27 *gag* region of SRV/D-1 to -5.

PCR results suggested that the N27 and T150 isolates are not SRV/D-4 or -5 but are closely related to SRV/D-1 to -5. Thus, we tentatively named the N27 and T150 isolates SRV/D-T. In order to characterize the SRV/D-T virus further, we sequenced the entire *gag* region of the N27 strain.

3.3. Comparison of the gag nucleotide sequence of SRV/D-Tsukuba with other SRV/D subtypes

Genomic DNA of N27 strain-infected Raji cells was prepared, and a 2189-bp fragment from the *gag* region of the integrated proviral DNA was amplified by PCR using the *gag* primer sets described in Section 2. Analysis of the amplified sequence revealed one large open-reading frame (ORF) (1980 bp; 659 aa). The sequence of the 1980-bp *gag* ORF of the N27 isolate was compared with the corresponding regions of SRV/D-1, -2 and -3 (Fig. 2). The nucleotide homology between the Tsukuba N27 isolate and other SRV/D strains varied from 78.5% to 81.1%, whereas the homology between SRV-1 and SRV-3 was 92.8% and the homology between SRV-1, -3 and SRV-2 was 79.2% and 79.6%, respectively (Table 1). Comparison of deduced amino acid sequences of the N27 isolate and other SRV/Ds gave similar results, suggesting that the N27 isolate is closely related to, but distinct from, the other known SRV/Ds (Table 1).

Since only a part of the *gag-prt* region of SRV/D-5 has been published (AF252389) [9], the corresponding region of the N27 strain (629 bp) was compared with that of SRV/Ds. Nucleic acid sequence homology between the N27 strain and SRV/D-1, -2, -3, and -5 in the *gag-prt* region was 83.5%, 83.0%, 82.8% and 84.1%, whereas the homology between N27 isolate and T150 strain was 99.7%.

In the *gag* region, five post-translational proteolytic products (p10, p12, p27, p14 and p4) have been reported for SRV/D-1, -2 and -3 [26,27]. Alignment of the deduced amino acid sequence of the N27 strain revealed that the probable proteolytic cleavage sites for each polypeptide are identical

Fig. 2. Alignment of amino acid sequences in the *gag* region of the SRV/D N27 isolate and SRV/D-1, -2, -3. The probable proteolytic cleavage sites for generation of the p10, p12, p27, p14, and p4 polypeptides are indicated.

Table 1
Percent homology of nucleic acid and amino acid sequences of the entire SRV/D *gag* region

Sequence	N27 vs SRV-1	N27 vs SRV-2	N27 vs SRV-3	SRV-1 vs SRV-2	SRV-1 vs SRV-3	SRV-2 vs SRV-3
Nucleic acid	81.1	78.5	80.6	79.2	92.8	79.6
Amino acid	86.2	82.9	85.9	84.0	96.2	84.3

Table 2
Percent homology of nucleic acid sequences of post-translational proteolytic products in *gag* genes

Region	N27 vs SRV-1	N27 vs SRV-2	N27 vs SRV-3	SRV-1 vs SRV-2	SRV-1 vs SRV-3	SRV-2 vs SRV-3
p10	92.0	91.0	92.0	92.0	100.0	92.0
p12	76.7	67.4	75.6	67.5	95.2	66.3
p27	97.4	95.2	96.5	96.0	99.1	96.0
p14	85.3	89.4	82.1	84.2	91.6	84.2
p4	83.3	88.9	83.3	88.9	100.0	88.9

(Fig. 2). Table 2 shows the high homology of p10 and p27 (91.0–100%) and the intermediate homology of p12 and p14 (66.3–95.2%) in all moleculary characterized SRV/Ds, including the N27 isolate. It is interesting that while the N27 isolate has greater homology to SRV/D-1 and -3 in the p10, p12 and p27 regions, it had significantly greater homology to SRV/D-2 in the p14 and p4 regions.

3.4. Phylogenetic analyses

The nucleotide sequence of the entire *gag* gene was analyzed to evaluate the phylogenetic relationship of the N27 strain with other known SRVs and related retroviruses based on sequences available from the GenBank database.

These analyses placed the new Tsukuba virus firmly in the SRV/D group (Fig. 3). While SRV/D-T was more closely related to SRV/D-2 than to SRV/D-1 and -3, the branch length separating N27 and SRV/D-2 was greater than that separating SRV/D subtypes 1 and 3. These, together with the varying degree of homology of individual *gag* derived proteins, indicate that the Tsukuba isolate represents a new subtype of SRV/D (Fig. 3).

4. Discussion

According to published observations on clinical findings, the outcomes of SRV/D infection can be divided into three categories: (a) no apparent clinical signs of disease or viremia with a high antibody titer, (b) low viremia and a transient antibody response with or without chronic disease, and (c) a high viremic state with rapid disease progression and no antibody response [28,29]. Cynomolgus monkeys from which SRV/D-T was isolated were seropositive for SRV/D but had no clinical signs of disease for several years. Thus, the two monkeys would belong to category (a). Based upon periodical health examinations and daily observations of these two monkeys, they were suspected of experiencing the onset of SAIDS (having anemia, weight loss, and persistent unresponsive diarrhea). At this time, blood samples were collected for virus isolation.

We are convinced that the virus isolates derived from the monkey PBMCs are a subtype of SRV/D based on the following evidence: (1) co-cultivated Raji cells showed typical SRV/D CPE, including syncytia (Fig. 1A); (2) RT activity was detected in the culture supernatant only after co-cultivation; (3) infected Raji cells were positive using anti-